Structure of soft-sphere dipolar fluids

Mark J. Stevens and Gary S. Grest
Corporate Research Science Laboratories, Exxon Research and Engineering Company, Annandale, New Jersey 08801
(Received 15 July 1994; revised manuscript received 15 February 1995)

We examine the structure of soft-sphere dipolar (SSD) fluids as a function of density and applied field. Besides being fundamental test systems for theory, dipolar fluids are models for ferrofluids. We show that chain formation is a fundamental characteristic of the SSD fluid resulting in a phase diagram much different from fluids with an isotropic potential. In particular, two-phase liquid-gas coexistence does not appear to occur in the absence of an applied field. In an applied field, phase coexistence does occur and we discuss the structure of the SSD system in the vicinity of the critical point. In contrast to expectations, the SSD does not model ferrofluids well. An additional attractive interaction beyond the dipolar interaction is needed to model ferrofluids.

PACS number(s): 61.20.−p, 83.80.Gv, 75.50.Mm

I. INTRODUCTION

A fundamental problem of statistical mechanics is the phase diagram of dipolar spheres. In contrast to simpler systems such as the Lennard-Jones (LJ) system, dipolar systems possess a long-ranged interaction that is attractive or repulsive depending on the orientation. Recent simulations [1–8] have shown that dipolar systems possess a rich variety of structures and a complex phase diagram. An understanding of the structure of dipolar systems will help in understanding model dipolar systems such as ferrofluids, magnetorheological (MR) fluids, and electrorheological (ER) fluids. Ferrofluids are permanent magnetic dipoles in solution. The MR and the ER fluids are similar except that the dipoles are not permanent, but induced. In addition, for ER fluids image dipoles must be treated. These systems combine the interesting behavior of magnetism or electricity with that of fluids yielding intriguing phenomena and technological applications [9,10]. In this paper we expand on results of our recent Monte Carlo (MC) simulations [8] of dipolar soft spheres in an applied field and examine the zero field phase diagram.

Recent simulations [1–8,11] modeled systems that have permanent dipole moments within the range found in ferrofluids. Two important findings have resulted from these simulations. The first is that at high densities a magnetic fluid phase can occur in the absence of an applied field [1,2]. Such a state is yet unattainable in the ferrofluid system, partly because the maximum attainable volume fraction of magnetic material is low (20%). The second important result is that for hard- or soft-sphere dipolar systems with purely repulsive short-range interactions, simulations have not found a two-phase liquid-gas coexistence in zero field [3,6,7]. This differs from experiments on ferrofluids in which phase coexistence is observed [12,13] and theories of dipolar systems that predict it [14–23]. These results, in conjunction with the simulations of van Leeuwen and Smit [7], who found that a dipolar interaction with some additional attraction does have phase coexistence, clearly demonstrate the significance of nondipolar attractive interactions. Therefore, there is a fundamental difference between dipolar systems with only a purely repulsive core and, for example, Stockmayer fluids, which have an additional LJ interaction besides the dipole interaction.

Our previous work found coexistence for soft-sphere dipoles in an applied field H [8]. The critical density ρ_c is approximately independent of H. Furthermore, ρ_c is at a rather low density and gives a lower bound for ρ_c at $H = 0$. Together with the simulations of van Leeuwen and Smit [7], which give an upper bound for ρ_c, our results show that coexistence can only occur, if at all, in a narrow density range and the dimensionless critical temperature must be significantly less than all predicted values.

The dipole-dipole interaction between particles i and j is

$$U_{dd}(\mathbf{r}_{ij}) = \frac{\mu^2}{r_{ij}^3}\left[\hat{\boldsymbol{\mu}}_i \cdot \hat{\boldsymbol{\mu}}_j - 3(\hat{\boldsymbol{\mu}}_i \cdot \hat{\mathbf{r}}_{ij})(\hat{\boldsymbol{\mu}}_j \cdot \hat{\mathbf{r}}_{ij})\right], \quad (1)$$

where $\boldsymbol{\mu}_i$ is the dipole moment of the ith particle, $\mathbf{r}_{ij}$ is the displacement vector between the two particles, and a caret signifies a unit vector. There are three relevant parameters for the dipolar systems: the density ρ, the dimensionless dipolar coupling strength given by the ratio $\lambda = \mu^2/\sigma^3 T$, where σ is the particle diameter and T is the temperature, and the dimensionless applied field $\eta = \mu H/T$. The temperature may also be an independent variable depending on the nondipolar interactions. In any case, the dimensionless temperature is $\tau = 1/\lambda$.

Some sort of repulsive core is necessary in order to remove the singularity of the dipolar interaction at zero separation and to model the steric repulsion. We use the soft-sphere potential, which commonly has the form

$$U_{\mathrm{SS}}(r_{ij}) = 4\varepsilon\left(\frac{\sigma}{r_{ij}}\right)^{12}, \quad (2)$$

where σ is the effective particle diameter and ε is the energy scale. For these soft-sphere dipoles (SSDs) the

core potential is purely repulsive and all attraction arises solely due to the dipolar interaction. Thus all condensation occurs because of the dipolar interaction. For hard-sphere dipoles, the temperature and λ are dependent quantities. Strictly speaking, this does not hold for the soft-sphere dipoles, but changing the temperature is basically equivalent to shifting the effective hard-sphere diameter and we can thus view the two quantities as dependent.

The other prototypical potential is the Lennard-Jones dipoles or the Stockmayer fluid [7,24,25]. In this system, along with the dipole potential there is a LJ potential

$$U_{\mathrm{LJ}}(r_{ij}) = 4\varepsilon \left[\left(\frac{\sigma}{r_{ij}} \right)^{12} - \left(\frac{\sigma}{r_{ij}} \right)^{6} \right]. \tag{3}$$

The LJ potential can be viewed as modeling the van der Waals interaction between the particles. In this case, attractive interactions arise from both the LJ and the dipolar interactions. The temperature and λ are now independent quantities in contrast to the SSD system. Unlike the SSD fluid, a liquid phase can occur solely due to the nonpolar interaction. In particular, the LJ system has a critical point at $T_c^* = 1.32$ and $\rho_c^* = 0.33$ [26], where variables are given in reduced form: $T^* = T/\varepsilon$, $\rho^* = \rho\sigma^3$, $\mu^{*2} = \mu^2/\varepsilon\sigma^3$, and $H^* = H\sqrt{\sigma^3/\varepsilon}$. The σ is either the soft sphere or the LJ diameter depending on the potential. Coexistence has been found for the Stockmayer system in zero field; at $\mu^* = 2$, the critical point is $T_c^* = 2.09$ and $\rho_c^* = 0.289$ [24].

Another difference between the Stockmayer fluid and the SSD fluid is that the former has a negative pressure at high densities for $\lambda \gtrsim 2$ [27]. Thus the Stockmayer fluid is unstable where the magnetic liquid phase occurs in the SSD system. For this reason the SSD system was favored in some simulations [1,2,8,28]. Not surprisingly, the values of ρ and λ, where negative pressures occur, turn out to be within the two-phase coexistence regime. The structure of the Stockmayer system at liquid densities in the one-phase regime has not been previously examined for the existence of a magnetic liquid phase. In the following paper [29], we calculate the coexistence curves for the Stockmayer system at larger values of μ^* (≥ 2.5) and find the magnetic liquid phase in the one-phase regime. Assuming that the phase is not a supercooled liquid, we find that at least for $\mu^* \geq 2.5$, the Stockmayer fluid, like the SSD fluid, has a magnetic liquid regime [29].

Van Leeuwen and Smit [7] recently examined the effect of varying the attractive part of the LJ interaction upon the critical point. They used the nondipolar interaction

$$U_{6\text{-}12}(r_{ij}) = 4\varepsilon \left[\left(\frac{\sigma}{r_{ij}} \right)^{12} - \epsilon_6 \left(\frac{\sigma}{r_{ij}} \right)^{6} \right], \tag{4}$$

where ϵ_6 is the constant used to vary the strength of the attractive interaction. As ϵ_6 decreases from 1, which is just the Stockmayer fluid, T_c and ρ_c decrease monotonically. However, for $\epsilon_6 \lesssim 0.30$ no coexistence was found.

As noted above, there have been several theoretical calculations of the critical point for hard-sphere dipoles [14–23,30]. All of these find phase coexistence in the absence of an applied field, in contrast to the simulations. Among these various theoretical calculations there is very little agreement on the value of either T_c or ρ_c. Values for the dimensionless critical temperature τ_c range from 0.225 to 0.66 and for ρ_c^* from 0.053 to 0.50 for $H = 0$. Two mechanisms have been proposed for coexistence. One is that fluctuating dipoles produce a van der Waals interaction and the traditional gas-liquid coexistence. In addition, a second coexistence mechanism occurs due to the magnetic fluid phase in which the isotropic-magnetic fluid transition ends in a tricritical point yielding coexistence between the isotropic and the magnetic fluids or at even lower temperatures between the gas and the magnetic fluid phases [22,30].

The ranges for ρ_c and T_c are quite large and suggest that many of the approximations are invalid. Furthermore, the simulations strongly suggest no coexistence in zero field and if a critical point exists, it is outside the predicted range. The failure of the theories of hard- or soft-sphere dipoles is the presumption that the fluctuating dipolar interaction yields a van der Waals interaction, which in turn leads to coexistence. We show below (Secs. III A and IV) that in the regime of interest, the dipolar interaction cannot be approximated by a van der Waals interaction. In the hard-sphere dipolar system condensation is induced solely by the dipolar interaction and the simulation results presented here show that the condensation is fundamentally different for dipoles with purely repulsive cores. In contast, in the Stockmayer system the van der Waals interaction is already present and induces a liquid phase. The coexistence that occurs in Stockmayer systems is a perturbation of normal gas-liquid coexistence of a LJ fluid. Not surprisingly, the Stockmayer fluid possesses coexistence within the range predicted.

In recent density functional calculations [30], it was found that the phase coexistence depends on the shape of the system volume. In these calculations, the system was taken as an ellipsoid of revolution with axis of revolution k times the other two axes. The magnetic fluid phase is favored for large k. Simulations with the Ewald sum usually treat a cubic, or equivalently spherical, system [31]. The cube has side length $S \gg L$, where L is the simulation box length. The simulation is generally viewed as modeling a microscopic piece of the bulk system. For example, with respect to ferrofluids, which are often experimentally studied confined between parallel plates, the simulation models a cube within the middle of the system. Ideally, one wants to choose the permeability due to the boundary conditions at S, μ_{BC} equal to the permeability of the bulk system μ_{bulk}, but that requires *a priori* knowledge, which one does not have. Recent simulations have shown that the difference between using $\mu_{\mathrm{BC}} = \infty$ and $\mu_{\mathrm{BC}} = \mu_{\mathrm{bulk}}$ is small as long as μ_{bulk} is large [2].

Here we present results of simulations on SSD systems examining the structure of systems with and without an applied field at four different values of the dipole moment. Simulations for the Stockmayer fluid in a field are presented in the following paper [29]. After describing the simulation model and method in Sec. II, we exam-

ine the fluid phase to determine the nature of the condensed phase contrasting it with that of the Stockmayer fluid. In particular, the onset of chain formation and the densed fluid structure is determined for a range of dipole strengths in Secs. III A and III B, respectively. We also determine in Sec. III C the magnetic fluid transition density for a range of dipole strengths. At high densities, we show and discuss a strong dependence on initial conditions. The structure in an applied field is examined near the critical point in Sec. III D. In Sec. IV we present the complete fluid phase diagram as a function of ρ and τ. Conclusions and a comparison with experimental systems are given in Sec. V.

II. SIMULATION METHODS

Our simulations follow that of Wei and Patey [1,2] and Kusalik [28,32]. We performed simulations for $\mu^* = 2.0$, 2.5, 3.0, and 4.0. Most simulations were at $T^* = 1$, although some, especially in an applied field, were performed at varying T^*. The Ewald sum is used to evaluate the dipole interaction in periodic boundary conditions with the convergence parameter $\alpha = 5.75$ and reciprocal vectors are summed to $10\pi/L$, where L is the length of the simulation cell. The Ewald sum contains a boundary term for the total potential energy

$$\frac{4\pi}{(2\mu_{\rm BC}+1)L^3}\mathbf{M}^2, \tag{5}$$

where $\mathbf{M} = \sum_i \mu_i$ is the magnetization. We use $\mu_{\rm BC} = \infty$, making the above term zero. This allows the uniformly magnetized state to occur. A value of $\mu_{\rm BC} = 1$ will lead to magnetic domains because this condition prevents the system from having a net magnetization [2]. This form of the Ewald sum treats a periodic lattice enclosed in a large sphere or cube [31]. These boundary conditions are consistent with experiments performed between parallel plates. For a crystal lattice, Griffiths [33] has shown that in the thermodynamic limit, there is no dependence on the boundary conditions.

Canonical constant volume ensemble simulations were performed mainly with $N = 256$ particles. Previous simulations [2] found insignificant differences between 256 and 864 particle simulations in zero field. For a cubic cell $N = 256$ is commensurate with a fcc lattice. Dipoles form a centered tetragonal (ct) lattice at high densities, which is incommensurate with the $N = 256$ cube [2,4]. We have thus performed some simulations with $N = 192$, which is commensurate with the ct lattice. The simulations ran for at least 10^5 MC cycles with each cycle comprised of an attempt to translate and rotate every particle. However, at some phase points long runs of 5×10^5 cycles were required. The particle step size was chosen to achieve about 50% acceptance. The rotation step was usually set so that the component of the new moment in the direction of the old moment was at most 0.2. This was done for most cases since the acceptance rate could not be lowered to 50%. The rotation step size was lowered below 0.2, when that would yield a 50% acceptance.

Most of our simulations used either an initial configuration of random positions and moments or the last configuration of a previous run (both increasing and decreasing density). We will discuss the various initial configurations and the dependence on them in Sec. III C.

Gibbs ensemble simulations were also performed to determine the coexistence curves in an applied field. Below the critical temperature the Gibbs ensemble directly gives the two coexistence densities at a given temperature [34,35]. For the Gibbs simulations, $N = 512$. The Gibbs simulations required at least 10^5 cycles; here each cycle included an attempt to move each particle once, 100 attempts to change the cell volume, and 500 attempts to exchange particles between the two cells. Only a small percentage of exchanges is accepted in these Gibbs simulations. Thus an extremely large number of attempts is needed to gather reasonable statistics. We have verified that both the pressure and the chemical potential are the same in the two cells. The pressure is calculated from the virial expression and the chemical potential is calculated from the overlap of the particle insertion and extraction energy distributions [26].

Our simulations in the Gibbs ensemble were performed with $H^* = 0.25$, 0.5, 1.0, and 2.0. For all of these fields we found coexistence and the critical parameters are given in Table I. For each field only a few points on the coexistence curve were obtained, because the critical temperatures τ_c are relatively low, making simulation times prohibitively long. For this reason, $H^* < 0.25$ were not studied. We determined τ_c by bracketing it between the Gibbs run that gave two clearly distinct densities, implying coexistence and the Gibbs run that gave a single-peaked density distribution implying that $\tau > \tau_c$. The uncertainty in τ_c, ± 0.008, comes directly from this bracketing. The critical density is taken from the law of rectilinear diameters. With just a few points estimating the uncertainty in ρ_c^* is difficult, but as ρ_c must be between the two coexisting phase densities, we estimate the uncertainty as ± 0.005.

We characterize the system structure through two order parameters [2]. The rank-one order parameter P_1 is defined as

$$P_1 = \frac{1}{N}\sum_{i=1}^{N} \hat{\boldsymbol{\mu}}_i \cdot \hat{\mathbf{d}} = \frac{1}{N}\mathbf{M}\cdot\hat{\mathbf{d}}, \tag{6}$$

where $\hat{\mathbf{d}}$ is the director and $\mathbf{M}$ is the total magnetization of the system. For a completely magnetized system, $P_1 = 1$. The second-rank order parameter P_2 is the largest eigenvalue of the matrix

TABLE I. Critical parameters at various field strengths.

H	ρ_c^*	λ_c	η_c	τ_c
0.25	0.032	8.93	0.82	0.112
0.50	0.032	6.94	1.40	0.144
1.0	0.030	6.44	2.60	0.155
2.0	0.035	5.95	4.75	0.168

$$Q_{\alpha\beta} = \frac{1}{N}\sum_{i=1}^{N}\frac{1}{2}(3\mu_i^\alpha\mu_i^\beta - \delta_{\alpha\beta}), \tag{7}$$

where μ_i^α is the α component of the unit vector $\hat{\boldsymbol{\mu}}_i$. The corresponding eigenvector is the director. For an ordered nematic state, $P_2 = 1$.

Either an applied field or high densities will orient dipolar systems and it is thus useful to examine the structure parallel and perpendicular to the preferred direction. To do this we calculated two pair distribution functions

$$g_\perp(r_\perp) = \frac{\left\langle \sum_{i,j\neq i} \delta(r_{ij}^\perp - r_\perp)\right\rangle}{N2\pi\rho r_\perp L}, \tag{8}$$

$$g_{||}(r_{||}) = \frac{\left\langle \sum_{i,j\neq i} \delta(r_{ij}^{||} - r_{||})\right\rangle}{N\rho L^2\Delta r_{||}}, \tag{9}$$

where L is the simulation box length, $r_{ij}^{||}$ and $r_{ij}^\perp$ are the parallel and perpendicular distances to the preferred direction, and $\Delta r_{||}$ is the bin width.

In order to examine the anisotropic order in the dipolar systems, we also calculated the two-dimensional pair distribution function $g(\varrho, z)$,

$$g(\varrho, z) = \frac{\left\langle \sum_{i,j\neq i} \frac{1}{2}[\delta(\varrho - \varrho_i)\delta(z - z_i] + [\delta(\varrho - \varrho_j)\delta(z - z_j)]\right\rangle}{N2\pi\rho\varrho\Delta z}, \tag{10}$$

where $z_i = \hat{\boldsymbol{\mu}}_i \cdot \mathbf{r}_{ij}$, $\boldsymbol{\varrho_i} = \mathbf{r}_{ij} - (\hat{\boldsymbol{\mu}}_i \cdot \mathbf{r}_{ij})\hat{\boldsymbol{\mu}}_i$, and Δz is the bin size for z. Given a particle at the origin with its moment along the z axis, the probability to find another particle with cylindrical coordinates (ϱ, z) is $g(\varrho, z)$.

III. RESULTS: STRUCTURE OF SOFT SPHERE DIPOLAR SYSTEM

A. Onset of chain formation

A gas phase must exist at sufficiently high temperatures and/or low densities. The transition to the liquid state occurs when particles begin to condense forming clusters. Usually, the onset of the liquid phase can be roughly determined from when the average number of particles per cluster is greater than 1. In this case the pair distribution function will exhibit peaks corresponding to the nearest-neighbor separation. In purely dipolar systems, the cluster structure is anisotropic. The nearest neighbor of a particle is most likely at either the dipoles' head or tail.

We performed a cluster analysis similar to that of Weis and Levesque [3]. Two particles are defined as bonded if their dipolar pair energy is lower than $u_{\text{bond}} = -1.5\lambda k_B T$. This choice corresponds to an intermediate state between the parallel and antiparallel states. Two collinear, parallel particles i and j can continuously go to the antiparallel state by rotating j about i and simultaneously rotating the moment of j. The dipole energy is $-1.5\lambda k_B T$ when the dipole moments are perpendicular and the angle between $\mathbf{r}_{ij}$ and $\boldsymbol{\mu_i}$ is $\pi/4$. Thus this energy range does not consider the antiparallel state as bonded since its dipolar pair energy is $-\lambda k_B T$. Pair energy distributions show that for large values of λ the antiparallel state is only a transient state. The clusters that form are linear chains and rings. We do allow branched chains in our formulations, but they occur rather rarely with this choice of cluster definition.

Some idea of the density dependence of the chain formation can be obtained from the virial coefficient, which has been calculated for large λ [15]. The asymptotic expression for the virial coefficient B is

$$B = -\frac{\pi\sigma^3}{18\lambda^3}e^{2\lambda}. \tag{11}$$

The density of dimers ρ_2 is $-B\rho^2$. The system would be all dimers at $\rho_2^{\text{all}} = -1/B$. Of course, trimers, etc., will form starting at a lower density and we should think of ρ_2^{all} as an upper bound for strong bonding. The key point is that the exponential dependence produces extremely small values for ρ_2^{all} at the typical values of λ. For $\lambda = 9$, this density is $\rho^* = 6.4 \times 10^{-5}$. Thus the virial implies a significant amount of chaining even at quite low densities.

Jordan [36,37] has performed an improved calculation of n-mer probabilities in the limit of large λ. He calculated the partition functions in both zero and nonzero fields treating only linear chains. The critical condition for chain formation is $\rho c \simeq 1$, where

$$c = \frac{4\pi\sigma^3}{81a_1\lambda^2}\exp[2\lambda\zeta(3)], \tag{12}$$

where $a_1 = 1 - 1/256$ and the Riemann zeta function $\zeta(3) = 1.202$ for $H = 0$. The exponential dependence on λ remains and the densities for the onset of chain formation for λ =4, 6.25, 9, and 16 are $\rho^* = 0.0069$, 4.5×10^{-5}, 2.1×10^{-7} and 3.2×10^{-14}, respectively, extremely dilute densities. From just these simple calculations we see that dipolar systems with a purely repulsive core possess a radically different phase diagram compared to the LJ system, for example.

One can do another simple calculation that indicates the density at which dipolar interaction become important in comparison with thermal fluctuations. We define the dipolar interaction length, much like the Bjerrum

length for Coulomb systems, to be the separation distance at which the dipole-dipole interaction energy equals k_BT:

$$\ell_B = \left(\frac{\mu^2}{k_BT}\right)^{1/3} = \lambda^{1/3}\sigma. \tag{13}$$

The dipole interactions will be significant at the density ρ_B, where the average particle separation equals ℓ_B. Taking the average separation distance to be $\rho^{1/3}$ we find

$$\rho_B^* = \lambda^{-1} = \tau. \tag{14}$$

Since for $\rho > \rho_B$ the dipole interactions between nearest neighbors is greater than k_BT, ρ_B is the density at which all particles will be part of a chain, if λ is large enough to produce a strong bond. Equation (14) also gives a connection between ρ and T, which suggests a boundary in the phase diagram (see Sec. IV).

Using our cluster analysis, we can test the above predictions. For $\lambda = 4$ we find that less than 0.5% of the particles are in dimers at $\rho^* = 0.01$. At this density no higher-order n-mers exist. By $\rho^* = 0.1$ the average number of particles per chain $\langle n \rangle$ is 1.04 or about 4% of the particles are in a dimer. The density dependence is logarithmically decaying and by $\rho^* = 0.001$ the number of dimers is practically zero. Thus chain formation begins at the same order of magnitude as given by the Jordan criterion. However, if we examine $g(r)$, a peak is found at the nearest-neighbor distance even at $\rho^* = 10^{-4}$ (Fig. 1). This peak is due to dimers, since no structure is observed at longer separations; the system is gaslike except for the peak at $r = \sigma$. To compare to the cluster analysis one must examine the number density $n(r) = \rho g(r)$. The area under the first peak gives the actual number of bonded dipoles. Because ρ is so small and the peak heights are of order 1 for $\lambda = 4$, the number of dimers implied by $g(r)$ becomes logarithmically small, even though $g(r)$ at $r = \sigma$ is quite large.

A more dramatic display of the large peaks in $g(r)$ is found for $\lambda = 9$. Because the peaks are so large, we plot $n(r)$ instead of $g(r)$ in Fig. 1. In both cases, higher-order peaks due to trimers, etc., are visible. The dimer peak is rather sharp and well defined. The dimer peak height for $n(r)$ is about 1, which implies that the peak height for $g(r)$ is about $1/\rho^*$, quite large for these low densities. In fact, the peak height in the structure factor $S(k)$ is also large. The peak height for $\lambda = 9$ at $\rho^* = 0.01$ is greater than 6. By the Hansen-Verlet criterion, such a peak height usually implies the system is a solid [38]. Obviously, this is not true. One can understand this in terms of the Hansen-Verlet criterion by realizing that the bonds that yield the first peak are extremely stable, i.e., solidlike. That the bonds are quite stable is also indicated by $n(r)$ being zero between the peaks.

There is an additional unusual characteristic of $g(r)$. One normally expects the first peak height to decrease with decreasing density and disappear as the gas regime is entered. In contrast to this trend, we find that the first peak actually grows with decreasing density for large λ, but the peak heights in $n(r)$ decrease with decreasing density as required. This increase in the peak height of

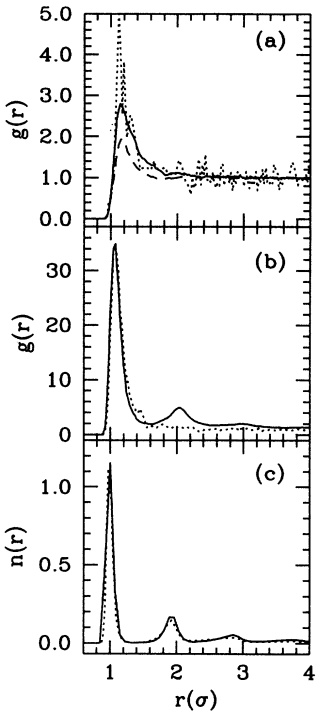

FIG. 1. Distribution functions at low densities show peaks due to chain formation: (a) $g(r)$ for $\mu^* = 2$ ($\lambda = 4$) at $\rho^* = 10^{-4}$, dotted line; $\rho^* = 0.01$, solid line; $\rho^* = 0.1$, short dashed line. (b) $n(r)$ for $\mu^* = 2.5$ ($\lambda = 6.25$) with same lines as in (a) except no $\rho^* = 0.1$. (c) $n(r)$ for $\mu^* = 3$ ($\lambda = 9$) with same lines as in (b).

$g(r)$ implies that the number of dimers does not decrease as rapidly as the density.

The degree of chaining at these low densities for high λ is exhibited in Fig. 2, which is a projection plot for $\lambda = 9$ at $\rho^* = 10^{-3}$. For these large λ values we always find strong chain formation even at such extremely low densities. Long chains containing up to 20 particles are shown in Fig. 2. Some of the chains have formed loops. We

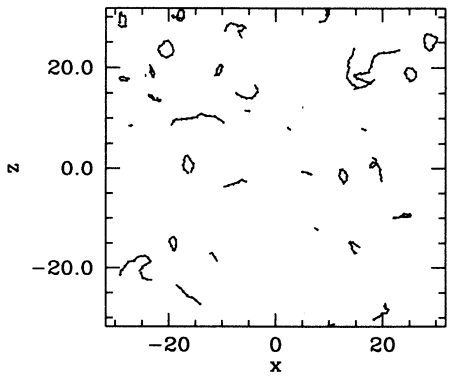

FIG. 2. Projection plot of $\mu^* = 3$ ($\lambda = 9$) at $\rho^* = 0.001$ shows the presence of chains and rings at an extremely dilute concentration.

cannot verify the Jordan criterion for the chain formation at $\lambda = 9$, since the onset occurs at about $\rho^* = 10^{-7}$. Clearly though, chain formation does occur at quite low densities for $\lambda \geq 9$.

We can compare our results with Jordan's criterion at $\lambda = 6.25$, which gives the onset at $\rho^* = 4.5 \times 10^{-5}$. At $\rho^* = 0.001$, 2% of the particles are in dimers according to the cluster analysis. By $\rho^* = 10^{-4}$, which is slightly above the Jordan density, 0.26% of the particles are in dimers. Extrapolations to $\rho^* = 1 \times 10^{-5}$ give about 0.02%, which is zero within error. Thus, for $\lambda = 6.25$ like $\lambda = 4$, Jordan's criterion appears to at least give the correct order of magnitude for the onset of chain formation.

An examination of $g(r)$ at low density for $\mu^* = 2.5$ shows the large peak due to the presence of dimers and even a small second peak for trimers at $\rho^* = 0.01$ (Fig. 1). Unlike the other cases, we find that the first peak in $g(r)$ at $\rho^* = 10^{-4}$ is lower than at $\rho^* = 10^{-3}$. Also in contrast to the larger λ behavior, all the peaks in $n(r)$ are less than one.

The chained structure of the SSD system at dilute densities is not at all like a LJ fluid. Gas-liquid coexistence for SSD was predicted on the basis of fluctuating dipoles interacting via a van der Waals potential. The chains that form at very dilute densities do not occur for van der Waals interactions. Both the structure and the lack of zero field coexistence in the SSD imply that something is wrong with the usual argument for the van der Waals coexistence. The derivation of the fluctuating dipole mean potential is only valid for $\lambda < 1$ [39], because it involves an expansion of the Boltzmann factor in powers of λ. In this regime, the dipole interaction is weak in comparison to $k_B T$ and the dipoles fluctuate considerably. However, outside this range, there are strong correlations in the dipole-dipole orientation, as our results show, and the average potential is no longer applicable.

The strong difference between the SSD fluid and the Stockmayer fluid is clearly exhibited in Fig. 3. The figure shows projection plots for both fluids for $\lambda = 4$ at $\rho^* = 0.01$ and $T^* = 1$. The Stockmayer fluid is in the coexistence region, as can be seen by the spherical droplets that have formed. In contrast there is no condensation present in the SSD fluid. Thus it is clear the condensation present in the Stockmayer fluid is due to the attractive part of the LJ interaction, which is consistent with spherical droplets forming instead of chains.

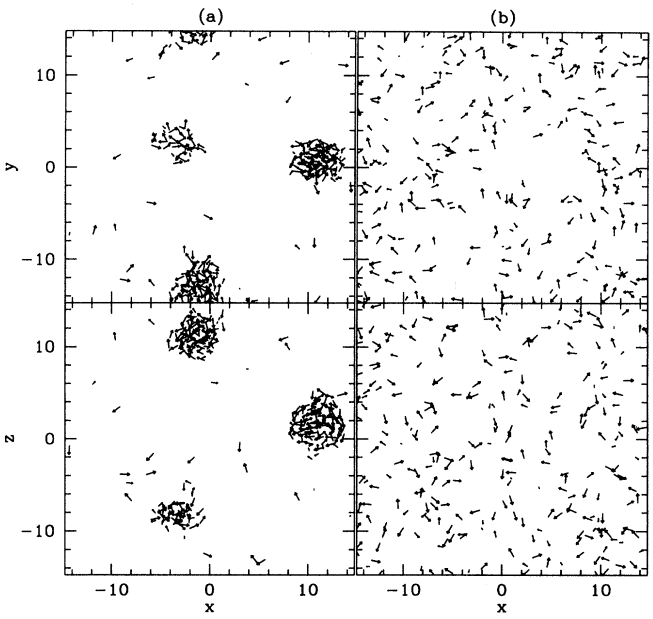

FIG. 3. Projection plots for (a) Stockmayer and (b) SSD fluids for $\mu^* = 2$ at $\rho^* = 0.1$ and $T^* = 1$ show the fundamental differences between the two systems' fluid structure.

B. Dense fluid phase

We now have some idea of the onset of chain formation and turn our attention to the structure of the chained fluid as a function of density and λ. In this section we consider the density regime in which the fluid is nonmagnetic.

At low densities the system is composed of chains of varying length that do not overlap. In the terminology of polymer physics, this is a dilute system. There will be an overlap density where the average chain-chain separation equals the average end-to-end distance of the chain. The value for the overlap density is difficult to determine because the chains are polydisperse and their length depends on density as well as λ. Beyond the overlap density the chains become entangled, greatly slowing the dynamics. However, unlike neutral polymers the dipolar chains have a tendency to orient and produce a nematic state. The structure of a dipolar fluid is thus more complicated than a polymer system.

We have seen that the structure of the SSD fluid at low densities differs greatly from the isotropic LJ fluid. This difference is due to the anisotropic dipole potential, which yields an anisotropic fluid structure (see Fig. 2). This anisotropy can be readily seen in the pair distribution function $g(\varrho, z)$. For $\mu^* = 3$ at $\rho^* = 0.01$ we show the surface plot of $g(\varrho, z)$ in Fig. 4. The most striking aspect

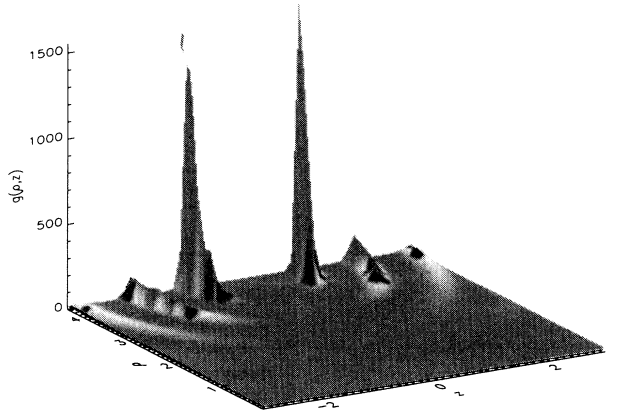

FIG. 4. The two-dimensional pair distribution function for $\mu^* = 3$ at $\rho^* = 0.01$ clearly displays the anisotropic structure of the fluid.

of the pair distribution function is the two large peaks corresponding to the high probability of parallel head-to-tail alignment of two dipoles. Instead of uniform rings at the successive neighbor distances, one finds smaller peaks that look like fingers but protrude further as one is farther from the origin. This distribution shows that the highest probability is along the z axis and that as the chains get longer, they also become more flexible.

The effects of chaining can be seen in the radial distribution functions as a function of density. Figures 5(a)–5(c) show $g(r)$ for $\mu^* = 2, 2.5$, and 3 at various densities in the range $\rho^* = 0.1$–0.7. In a system with an attractive interaction, the nearest-neighbor peak is located close to the position of the potential minimum and all the peaks grow as the density increases. The figures show that the nearest-neighbor peak for the SSD system is also located close to the position of the potential minimum. In all cases, the lowest density plotted has the highest first peak, continuing the trend noticed earlier for very dilute densities. Since the peak height is larger for larger λ, the trend is most noticeable for $\mu^* = 3$ for which $\rho^* = 0.1$ also has the highest second and third peaks. For $\mu^* = 2$, the peak heights increase with density for $\rho^* \geq 0.4$ as an isotropic fluid. For $\mu^* = 2.5$ the first peak height decreases until $\rho^* = 0.5$. In contrast, the first peak is always decreasing with density for $\mu^* = 3$. In fact, there are several differences between the $\mu^* = 2.5$ and $\mu^* = 3$ fluids.

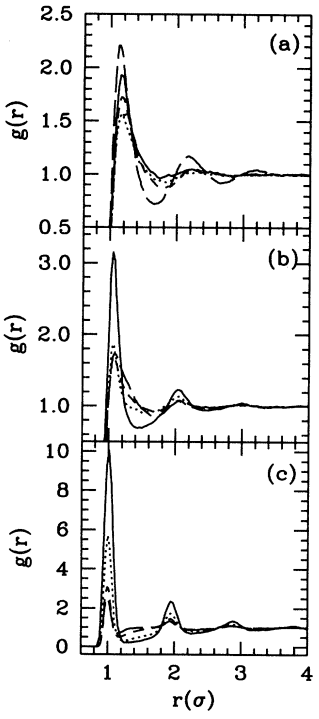

FIG. 5. Radial distribution functions at isotropic fluid densities for (a) $\mu^* = 2$, $\rho^* = 0.1$ (solid line); $\rho^* = 0.4$ (dotted line); $\rho^* = 0.5$ (short-dashed line); $\rho^* = 0.7$ (long-dashed line). (b) $\mu^* = 2.5$, $\rho^* = 0.2$ (solid line); $\rho^* = 0.4$ (dotted line); $\rho^* = 0.5$ (short-dashed line); $\rho^* = 0.6$ (long-dashed line). (c) $\mu^* = 3.0$, $\rho^* = 0.1$ (solid line); $\rho^* = 0.2$ (dotted line); $\rho^* = 0.4$ (short-dashed); $\rho^* = 0.5$ (long-dashed line).

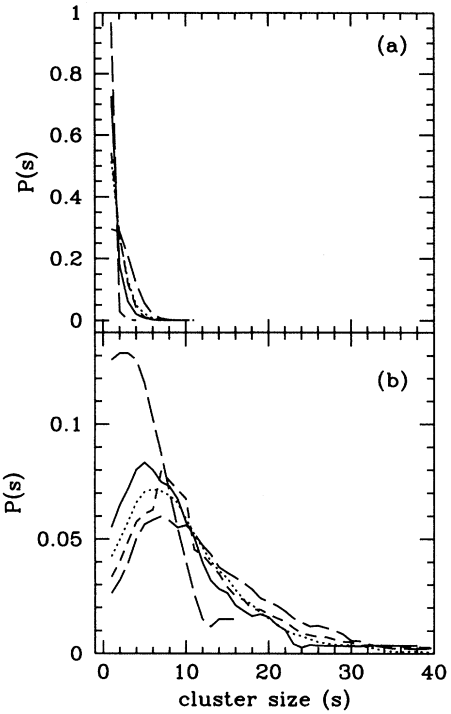

FIG. 6. The probability $P(s)$ of a particle being in a chain of size s is plotted for (a) $\mu^* = 2.5$ at $\rho^* = 0.001$ (long-dashed line), $\rho^* = 0.01$ (solid line), $\rho^* = 0.2$ (dotted line), $\rho^* = 0.7$ (short-dashed line), $\rho^* = 0.9$ (long-dashed line) and (b) $\mu^* = 3$ at $\rho^* = 0.001$ (long-dashed line), $\rho^* = 0.01$ (solid line), $\rho^* = 0.4$ (dotted line), $\rho^* = 0.6$ (short-dashed line), and $\rho^* = 0.7$ (long-dashed line).

At $\mu^* = 3$ most of the particles are contained in chains, as can be seen in Fig. 2. In contrast, most of the particles are in the monomeric state for $\mu^* = 2.5$ at all densities within the isotropic regime. From our cluster analysis, we calculate the probabiblity $P(s)$ of finding a particle in a chain of size s. We plot $P(s)$ in Fig. 6 at several densities for $\mu^* = 2.5$ and 3.0. This plot clearly shows the different degree of chaining between $\mu^* = 2.5$ and $\mu^* = 3$. The peak chain size for $\mu^* = 3$ varies in the range 5–10, except at $\rho^* = 0.001$, where the peak is at $s = 2$. The odd peak for $\mu^* = 3$ at $\rho^* = 0.6$ is due to chains preferring to be the same length as the simulation cell. The distributions will change slightly as u_{bond} is changed. However, changing u_{bond} by 20% does not alter the qualitative features of the distributions. Furthermore, the physical correspondence with our choice of u_{bond} implies certain structures upon the distributions. For $\mu^* = 2.5$ the particles are either well separated or the moments are not correlated. At the low densities, the smaller peak height and the nonzero values between peaks in $g(r)$ (Fig. 1) shows that the particles are much less bound than at $\mu^* = 3$. At high densities where the particles must be close, the distributions for $\mu^* = 2.5$ imply that the dipole moments do not become highly correlated until the transition to the magnetic fluid state.

Between $\mu^* = 2.5$ and 3, the dipole interaction becomes sufficiently strong that well defined, long lived molecules exist. At smaller μ^* the chains tend to be short and weakly stable. The $g(r)$ for $\mu^* = 3$ at low densities (Fig. 1) resembles a molecular $g(r)$ with sharp peaks due to the bonded atoms. One could separate $g(r)$ into intra- and interchain parts. Another characteristic that occurs for $\mu^* = 3$ but not for $\mu^* = 2.5$ is ring formation. Rings tend to be highly stable in comparison with linear chains, because to remove a particle from a ring requires breaking *two* bonds. The chains are not long enough at $\mu^* = 2.5$ for rings to occur.

At $\mu^* = 4$ chain formation is so stable that for $\rho^* \geq 0.1$ a set of chains is formed that never breaks. Thus one has severe ergodicity problems for simulations at this μ^*, particularly because the set of chains depends strongly on the initial configuration. Since the largest chain length tends to contain about half the total particles, we cannot say that we have equilibrated runs at $\mu^* = 4$. Even if we used a much larger system, the dynamics will be similar to that of a living polymer, which is much slower than a particle system.

C. Phase transition

For $\mu^* = 3$ at $T^* = 1.35$ ($\lambda = 6.67$) and $T^* = 1$ ($\lambda = 9$), Wei and Patey [2] calculated the order parameters P_1 and P_2 as a function of density starting from randomly oriented dipoles on a fcc lattice. They found a transition to a magnetically ordered state at $\rho^* \approx 0.65$ for $\lambda = 6.67$ and at $\rho^* = 0.60$ for $\lambda = 9$. At higher ρ^* the system exhibit smectic order and then (magnetic) solid order [2,5]. We discuss below our results for P_1 and P_2 for the four μ^* values discussed above.

We have performed simulations with a variety of starting states and have found some dependence on the initial configuration for $\mu^* \geq 3$. The initial state dependence for $\lambda = 9$ and 16 turned out to be due only to the orientation of the dipoles, random or oriented. The results were independent of the initial particle configuration. It did not matter whether it was initially a fcc lattice, a random configuration, or the last configuration from the previous lower density. Random dipole orientations are obtained by initially choosing random orientations. These runs do not differ from sequential runs of increasing density. In this case the low density dipolar orientation is sufficiently random. Oriented states are obtained by starting with all the moments parallel to the z axis. Similar to above, consecutive runs decreasing in density where the first run is at an ordered density with $P_1 > 0.5$ give the same results as when the moments are initially aligned.

We show results for P_1 and P_2 in Fig. 7 for four values of μ^*. The circles represent random dipole moments and the squares represent oriented moments. For $\mu^* = 2$ and $\mu^* = 2.5$ there is no dependence on these various starting states. Magnetic (nematic) ordering occurs for $\mu^* = 2$ at $\rho^* \simeq 0.85$ and for $\mu^* = 2.5$ at $\rho^* \simeq 0.67$ for $N = 256$. Since we were unable to perform long runs for large N, it is not possible at this time to determine finite corrections to these densities.

We found strong initial configuration dependence at $\mu^* = 3$ and 4. We tried a variety of starting states and, as stated above, found that the order parameters and thermodynamic quantities depend only on the dipole orientation. For initial states with a random orientation we obtain the same transition density as Ref. [2]. However, near the transition for $\mu^* = 3$, we found that extremely long runs (5×10^5 MC cycles) were required to achieve equilibrium from an oriented state. Runs of order 1×10^5 MC cycles appeared equilibrated in energy, but not for the order parameters. For $\mu^* = 3$, Fig. 7(c) shows some hystersis in the order parameters. At $\rho^* = 0.5$ the descending sequence of runs give an ordered state, but the ascending sequence gives an isotropic state.

For $\mu^* = 4$ an even stronger initial configuration dependence was found [Fig. 7(d)]. The magnetic fluid phase was not observed when the initial configuration had random dipole orientation. A sequence of runs starting from the high density oriented state gives the magnetic fluid transition at about $\rho^* = 0.1$. On the other hand, P_2 gives a transition near $\rho^* = 0.5$. As pointed out above, the cluster analysis shows that the system is composed of a few large chains, usually loops, which are not broken within the MC run and thus there are ergodicity problems. The plot of the order parameters clearly shows the extent of the initial state dependence. Because of this problem, we cannot determine the transition density for $\mu^* = 4$ beyond saying that transition satisfies $\rho^* \gtrsim 0.1$.

In this work we have not attempted to precisely determine the transition densities. Simulations for varying system size have not been performed to determine finite size effects. Previous simulations at $\mu^* = 3$ [2] found very little difference between $N = 256$ and $N = 864$ in P_1 and P_2 at selected densities. Although the size dependence was not examined close to the transition density, these simulations do indicate that the transition density will not vary by more than $0.1\sigma^{-3}$.

D. Field dependence

Previously, we had shown that in an applied field phase coexistence does occur for the SSD system [8]. We calculated the critical points at four fields $H^* = 0.25$, 0.5, 1.0, and 2.0 at $\mu^* = 2.5$ and found that $\rho_c^* \approx 0.03$ in all four cases. We reproduce the table of the critical data in Table I. The surprising aspect of the coexisting phases is that both phases contain predominantly long chains. In Fig. 8 we show the Gibbs coexisting densities for $H^* = 1.0$. As these runs take about 10 times the number of MC cycles than zero field Stockmayer Gibbs simulations, we could only calculate a few points. These few points are sufficient to give reasonable values of T_c and ρ_c, in part because the values are so low. Besides the three temperatures at which coexistence was found in Fig. 8 we also ran at $T^* = 1.1$ and found no coexistence. As mentioned above, T_c^* is determined from bracketing between T^* at which coexistence is and is not found.

The structure of the coexisting phases does not correspond to either of the theoretical pictures. Since chain-

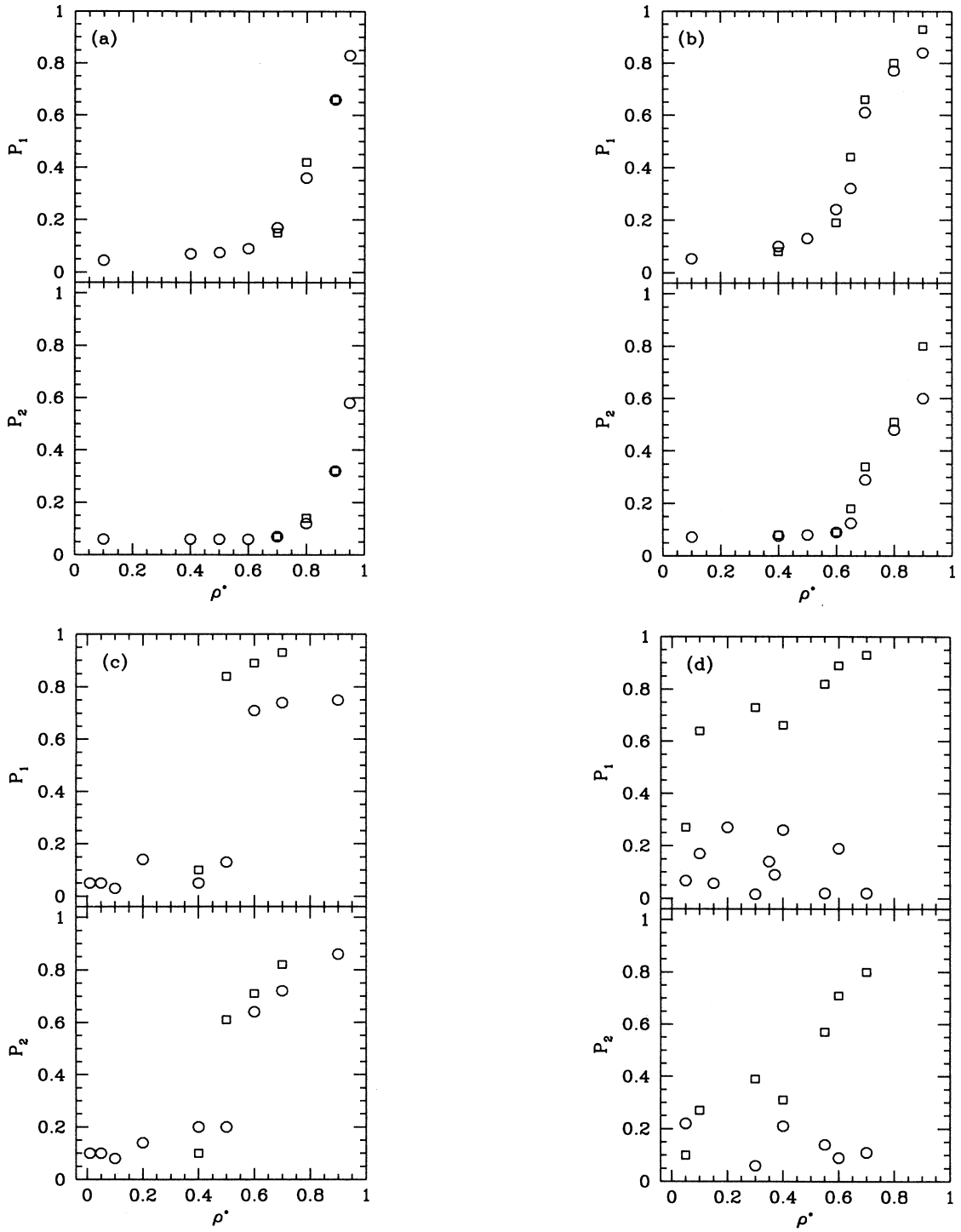

FIG. 7. Order parameters P_1 and P_2 for (a) $\mu^* = 2$, (b) $\mu^* = 2.5$, (c) $\mu^* = 3$, and (d) $\mu^* = 4$. The circles are for a random initial dipole moment orientation. The squares are for initially parallel dipole moments.

ing is significant in both phases, the phase coexistence is definitely not a gas-liquid coexistence. Both phases are magnetic which rules out the isotropic-magnetic (I-M) coexistence. However, it is possible that in the limit of $H \to 0$, the coexistence may become of the I-M type. The I-M transition occurs at much higher densities for the four μ^* values examined here, but (see also Sec. IV) the transition density is decreasing with increasing λ and such a convergence cannot be excluded.

Since both coexisting phases are chained, we want to confirm the equilibriation of the runs. In Fig. 9 we show for $H^* = 0.5$ and $T^* = 0.85$ the cumulative average pres-

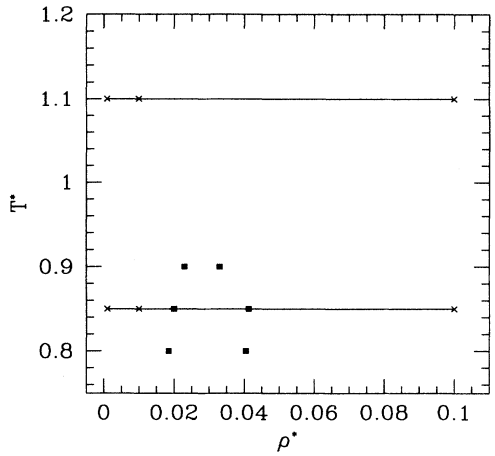

FIG. 8. Coexistence data for $H^* = 1.0$ (solid points). The Gibbs run at $T^* = 1.0$ gave no phase coexistence. The points and lines at $T^* = 1.1$ and $T^* = 0.85$ show where the canonical runs were done.

sures and the function $y(u) = T \ln[\rho f(u)/g(u)]$, where f and g are the test and the real particle energy distributions [26]. The pressures are calculated from the virial and Fig. 9(a) shows that the pressures are converged and equal. The slope of $y(u)$ should be 1 and the intercept gives the chemical potential. As usual, the slope of $y(u)$

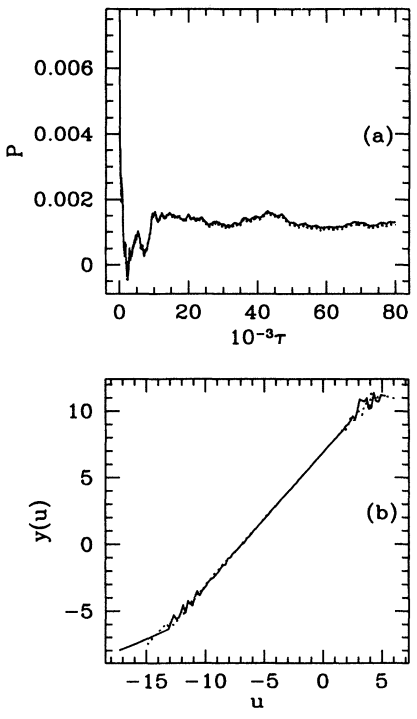

FIG. 9. Plots of (a) the cumulative average pressures and (b) energy distributions for both cells confirm that the pressures and chemical potentials are equal. τ is the number of MC cycles. The y intercept of the function $y(u)$ given in the text is the chemical potential.

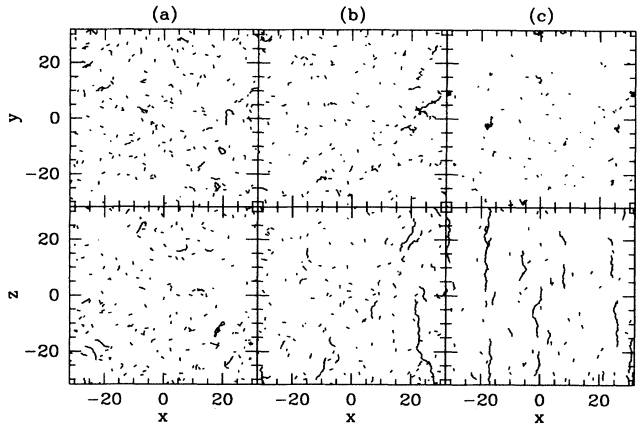

FIG. 10. Projection plots for $\mu^* = 2.5$ at $\rho^* = 0.001$ and $T^* = 0.85$ for $H^* = 0$, 0.5, and 2. The arrow length as drawn is 1σ.

deviates from 1 at low and high u where the sampling is poor. However, for several decades two straight, overlapping lines of unit slope occur, showing that the chemical potentials are equal.

We now present some results of canonical simulations in nonzero field. We would like to understand the nature of both coexisting phases, the effect of an applied field and the zero field limit. Canonical simulations in an applied field were performed in the vicinity of a critical point. Two sets of simulations were performed at constant T and $H^* = 1.0$. These runs are labeled in Fig. 8. One set of runs is performed at $T^* = 1.1 > T_c^*$ and the other at $T^* = 0.85 < T_c^*$. Simulations were also performed at constant density, varying the applied field. We report the results of two sets of these simulations: at $\rho^* = 0.001$ (below ρ_c) and $\rho^* = 0.1$ (above ρ_c).

Figures 10 and 11 show projection plots for $\rho^* = 0.001$ and $\rho^* = 0.1$, respectively. These simulations were performed at $T^* = 0.85$ and $\mu^* = 2.5$, which gives $\lambda = 7.35$. For $H = 0$, at this λ, chains already exist in the dilute phase at $\rho^* = 0.001$. An applied field tends to align the dipole moments parallel to the field yielding chains

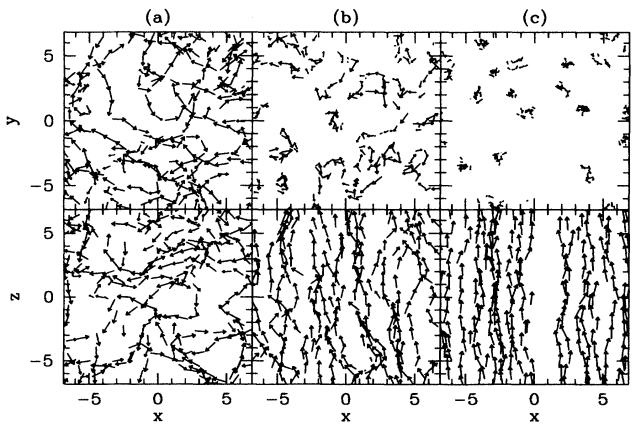

FIG. 11. Projection plots for $\mu^* = 2.5$ at $\rho^* = 0.1$ and $T^* = 0.85$ for $H^* = 0$, 1, and 10.

parallel to the field (z direction). The order parameter $P_1 = 0.59$ at $H^* = 0.5$ or $\eta = 1.47$, which implies that the dipoles are predominantly aligned with the field. However, Fig. 10(b) shows the chains do not necessarily align with the field. For this case $\eta < \lambda$; thus the local dipolar field dominates the applied field and the chains need not align with the field. Figure 10(c) shows the case where $\eta > \lambda$ ($H^* = 1$) and $P_1 = 0.97$. Here the long chains are directed along the field direction, although the chains are flexible and have local fluctuations away from the field direction.

Figure 10 also clearly shows that as H increases the chains grow. By $H^* = 10$, the system is composed of several long chains along with a few monomers. This picture of growing chains at dilute concentrations is similar to those seen in Fig. 1 of Ref. [40], which are photographs of ER fluids with $\lambda = 31$ and $\rho = 0.0047$. The chains are quite straight since the ER fluid has only induced dipoles.

At $\rho^* = 0.1$ the system is sufficiently dense that the zero field chains overlap (Fig. 11). At this higher density the chains orient parallel to the field at a much smaller field strength than the dilute density; at $H^* = 0.1$, $P_1 = 0.50$. The most striking aspect of the figure is chain alignment with the field, which results in a separation of the chains. By $H^* = 1$ the chains no longer overlap because they are oriented parallel to the field. Increasing the field makes the chains stiffer; their extent in the xy plane decreases considerably.

One possible explanation for the two coexisting chained phases is that one is a gas of chains and the other is a liquid. However, the xy projection at $H^* = 10$ and $\rho^* = 0.1 > \rho_c^*$ shows what appears to be a gas phase of chains. The calculated $g_\perp$ and $g_{||}$ for this density as a function of the applied field are shown in Fig. 12. A peak at $r = 0$ grows with the field in $g_\perp$. This peak is just the intrachain peak and shows the increase of the chains parallel to the field. There are no other peaks, suggesting the structure of the system is a gas of chains. The fact that the individual chains show no sign of clustering to form a column is an important difference from some experiments. Experiments on ferrofluids [41] and MR fluids [42–44] exhibit columns, not single chains. For ferrofluids it is not possible to discern single chain columns, but they may exist under some circumstances. On the other had, MR fluid can be imaged at the single-particle size and chains agglomerate into columns via a "zippering" action [42,43]. Such behavior is not present in the SSD fluid. This suggests that the agglomeration is an effect of attractive interactions not included in the SSD potential. One other possiblity is the flexibility of the chains in the SSD system presents an effective repulsive interaction for chain clustering. In MR fluids the chains are rather inflexible, because the dipoles are induced and are always parallel to **H**.

The projection plots in Fig. 13 show a continuous change as the density increases for $T^* = 1.1 > T_c^*$. At $\rho^* = 0.001$ [Fig. 13(a)] the system is mainly composed of dipoles that tend to point in the z direction ($P_1 = 0.60$) since $\eta = 2.3$. Figure 13(b) shows clustering present at $\rho^* = 0.01$, which is still in the less dense regime. By $\rho^* = 0.1$ [Fig. 13(c)] more clustering into chains has occurred. The chaining is rather weak, especially in comparison with the same density at $T^* = 0.85 < T_c^*$ [cf. Fig. 14(c)].

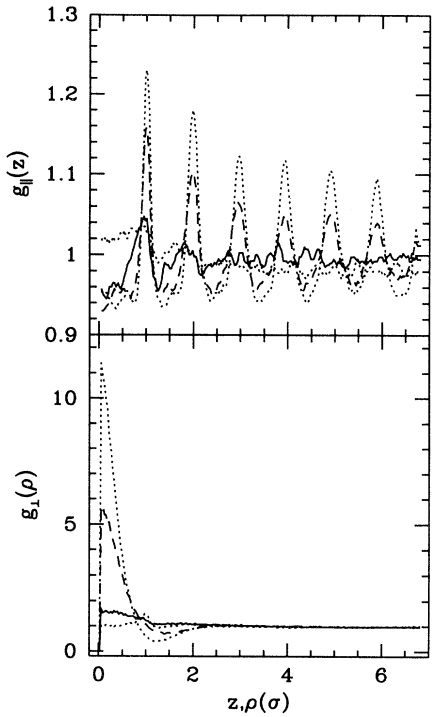

FIG. 12. Calculated $g_\perp(z)$ and $g_{||}(\rho)$ for $\mu^* = 2.5$ at $\rho^* = 0.1$ and $T^* = 0.85$. The solid line is $H^* = 0$, long-dashed line is $H^* = 0.25$, the short-dashed line is $H^* = 2.0$, and the dotted line is $H^* = 10$. The abscissa for $g_\perp$ is z and for $g_{||}$ is ρ.

In Fig. 14 we show the same densities as above but at $T^* = 0.85 < T_c^*$. Chaining is strongly present even at the very dilute density $\rho^* = 0.001$. These two figures show that decreasing T has effects similar to those resulting from increasing H. Chains grow and tend to be oriented

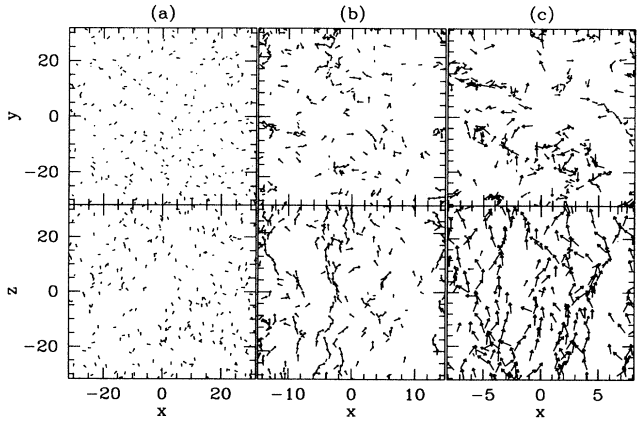

FIG. 13. Projection plots above T_c for $\mu^* = 2.5$ at $T^* = 1.1$ and $H^* = 1$. The densities are (a) $\rho^* = 0.001$, (b) 0.01, and (c) 0.1.

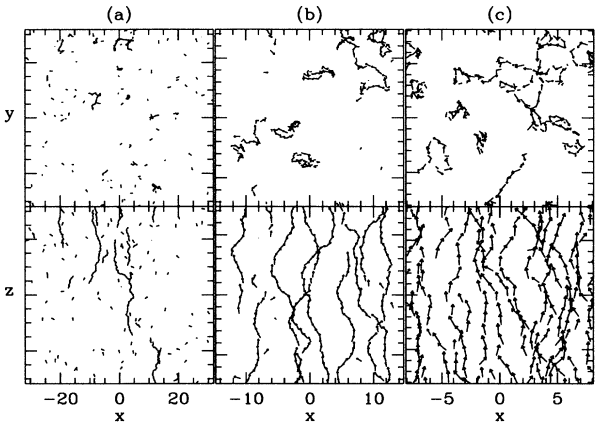

FIG. 14. Same as Fig. 13 but at $T^* = 0.85 < T_c^*$.

more parallel to **H**. Unfortunately, none of this gives us an indication of the difference between the two coexisting phases.

IV. PHASE DIAGRAM

We plot in Fig. 15 a partial phase diagram for the SSD system. The liquid-solid transition and any liquid-liquid transition such as the nematic-smetic transition are not included. The solid points represent the isotropic-magnetic fluid transition. The squares are our data and the triangles are from Ref. [2]. The open square for $\lambda = 9$ represents the transition density found for this λ using the decreasing density sequence. The arrow shows the

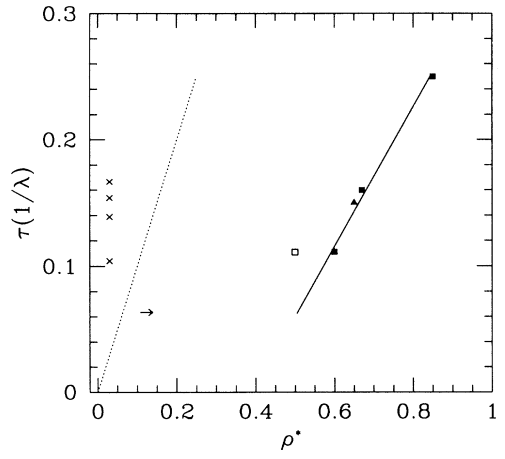

FIG. 15. Phase diagram for soft-sphere dipolar fluids. A description of the figure is given in the text in Sec. IV. The solid points (triangles [2] and squares, this paper) are the isotropic-magnetic fluid transition densities. The solid line is a least-squares fit to the solid points. The open square for $\lambda = 9$ represents the hystersis found for this λ. The arrow gives the lower limit on the transition density for $\lambda = 16$. The crosses are the critical points found in an applied field [8]. The dotted line represents the line $\rho_B^* = \tau$, Eq. (14).

lower limit on the transition density for $\lambda = 16$, which possesses strong nonergodic effects. The crosses are the critical points found in an applied field [8]. With increasing critical temperature the fields are $H^* = 0.25$, 0.5, 1.0, and 2.0. The dotted line represents the line $\rho_B^* = \tau$, Eq. (14). For $\rho^* > \rho_B^*$ the fluid is strongly interacting. The solid line is a least-squares fit to the solid points, which rather interestingly is a good fit. The extrapolation of this line to $\lambda = 16$ gives $\rho^* = 0.5$ and $\lambda = 0$ gives $\rho^* = 0.4$.

An interesting question is what happens to the *I-M* transition density ρ_{IM} as $\lambda \to 0$. Calculation of the mean field $\lambda = 0$ limit for hard spheres gives $\rho^* = 0.56$ [45]. This value is high, but if we equate this value with the extrapolated $\lambda = 0$ density, then the effective hard-sphere diameter is 1.1σ, which is only slightly larger than the soft-sphere diameter σ and is about equal to $r = 2^{1/6}\sigma \simeq 1.12$, where the value of U_{SS} is ϵ. The value of ρ_{IM} for $\lambda = 9$ from oriented simulations suggests a curving of the transition line toward much lower densities. Possibly, ρ_{IM}^* may be near 0.03 for very large λ and merge with the nonzero field phase coexistence.

We pointed out earlier (Sec. III A) that the approximation of dipole interaction as van der Waals interaction is valid only for $\lambda < 1$, yet this does not rule out phase coexistence. By examining the actual form of the van der Waals interaction, we find that in general, T^* is well above T_c^* in the relevant regime. The van der Waals form for the average dipole-dipole interaction [39] with a soft-sphere core has as the *total* potential $U_{6\text{-}12}$, where

$$\epsilon_6 = \lambda^2 T^*/3 = \mu^{*4}/3T^*. \tag{15}$$

To satisfy $\lambda < 1$, we must have $\epsilon_6 < T^*/3$ and $\epsilon_6 < \mu^{*2}/3$. For $\epsilon_6 = 1$, this implies $T^* > 3$ and $\mu^* > \sqrt{3}$. Thus $T^* > T_c^* = 1.3$ for $\epsilon_6 = 1$. At the lower value of $\epsilon_6 = 1/3$, the requirements are $T^* > 1$ and $\mu^* > 1$. Again, $T^* > T_c^* \simeq 0.17$ [7]. At smaller values of ϵ_6 phase coexistence does not occur.

V. CONCLUSION

We now have a picture of the SSD structure as a function of density for a broad range of dipole moments. The key component of the fluid structure is chains even at very dilute densities. The SSD fluid is much like a living polymer with a polydisperse distribution of chain sizes that is time invariant. For small λ, the chains break up easily, although for large λ the bonds become very stable as we see at $\lambda = 16$ for $\rho^* \gtrsim 0.1$. The anisotropy in the dipole potential that yields the chaining fundamentally effects the phase diagram. The structures that form are much more complex than, say, in the LJ system.

The SSD, as a simple dipolar system with a repulsive core, was thought to be a good model for ferrofluids and, with an induced dipole potential, good for the MR and the ER fluids. However, as this work shows, there are basic differences between this model and experimental systems. In particular, phase coexistence does not occur for the SSD in the absence of a field and while chains form, they do not coalesce into columns. In order to un-

derstand how to better model the experimental systems, we discuss them in more detail.

Experimentally, two types of ferrofluids have been studied for coexistence [12,13]. The difference is in the mechanism used to stabilize the particles against agglomeration due to the van der Waals interactions. This is done is either by coating the particles with a surfactant [13] or by using charged magnetic particles in an ionic solution [12]. In both cases, phase coexistence occurs in zero external field. More measurements have been performed on the ionic ferrofluids, which via added salt allow easier modification of the stabilization force than those stabilized by coating. In the absence of a field, neither the isotropic-magnetic fluid coexistence nor even a zero field magnetic fluid phase has been found. The volume fraction for the magnetic core can only be made up to 20% of fluid volume. At this fraction, the total particle volume fraction (including the core and the surfactant layers) is near close packing, limiting the maximum value of λ that can be achieved.

Modeling the ionic ferrofluids appears to be rather complex. The basic effect of the charges is to produce a repulsion between the magnetic particles. However, modeling these interactions is nontrivial because the charges on the particles are of order 10^4 and the simple Debye-Hückel model is not valid. The charges can also effect the phase coexistence, for even a simple electrolyte has phase coexistence [46]. Comparison of predictions based on the Stockmayer fluid [47] with experiment [12] show that polydisperisity plays an important role.

Coexistence for both types of ferrofluids occurs even in the absence of an applied field. Here we consider only the surfactant coated ferrofluids, which have been considered simpler to model. The coexistence curve as a function of field versus density for surfactant coated ferrofluids has been measured at two temperatures [13]. We identified these data incorrectly as critical points in a Letter [8], but the fundamental points remain the same. For the hydrocarbon based ferrofluid at 27 °C, $\rho_c^* \simeq 0.05$ is small, as in our simulations [8]. However, $\tau_c \simeq 1.0$ is much larger than our simulation value. Increasing the temperature raises the coexisting field and appears to increase ρ_c. Since the experimental system is highly polydisperse, the values of η_c and τ_c are average, but the difference in τ_c is too large to be ascribed to the polydispersity.

The surfactant ferrofluid has been simply modeled as a dipolar interaction plus a simple repulsive core that gives the particles their size. However, the results of these and recent simulations [7] suggest that modeling the stabilization interactions (and thus the van der Waals interaction) requires more than just a repulsive core. A better understanding of the nondipolar interactions is needed. Some attractive interaction must exist for coexistence in the absence of a field to occur. In the 6–12 potential, increasing ϵ_6 raises T_c as is needed to match experiment. However, this also raises ρ_c, which needs to be lowered. Given that many experiments are performed in an applied field, simulations in an applied field for the 6–12 potential that determine T_c and ρ_c would be very useful to compare to experiments. Such simulations are discussed in the following paper [29].

At the particle level, the structure of ferrofluids has hardly been probed [48]. The chaining of dipolar particles especially in an applied field has been observed, but not on the scale of individual particles [41]. In these experiments, droplets condense to form "chains." One can imagine the droplets in Fig. 3(a) in an applied field becoming magnetized and then coalescing to form columns. One means of probing individual particle interactions is to examine MR fluids, which are much larger than ferrofluids, although they posses only induced dipole moments. Additional advantages are the good monodispersity and high values of η (of order 100) that can be obtained. Because these particles diameters are about 1 μm, the systems can be probed through video microscopy [42,49]. Experiments on MR fluids between parallel plates show only column formation, except for very small plate separation (about 10σ). Initially, single-particle-thick chains are formed, which then form columns via a zippering action [42,43]. The column structure may very well be a solid structure, which implies that one of the coexistence phases is solid.

[1] D. Wei and G. Patey, Phys. Rev. Lett. **68**, 2043 (1992).
[2] D. Wei and G. Patey, Phys. Rev. A **46**, 7783 (1992).
[3] J. Weis and D. Levesque, Phys. Rev. Lett. **71**, 2729 (1993).
[4] J. Weis and D. Levesque, Phys. Rev. E **48**, 3728 (1993).
[5] D. Levesque and J. Weis, Phys. Rev. E **49**, 5131 (1994).
[6] J.-M. Caillol, J. Chem. Phys. **98**, 9835 (1993).
[7] M. van Leeuwen and B. Smit, Phys. Rev. Lett. **71**, 3991 (1993).
[8] M. J. Stevens and G. S. Grest, Phys. Rev. Lett. **72**, 3686 (1994).
[9] R. Rosensweig, *Ferrohydrodynamics* (Cambridge University Press, Cambridge, 1985).
[10] T. Halsey, Science **258**, 761 (1992).
[11] J. Weis, D. Levesque, and G. J. Zarragoicoechea, Phys. Rev. Lett. **69**, 913 (1992).
[12] J.-C. Bacri *et al.*, J. Colloid Interface Sci. **132**, 43 (1989).
[13] R. Rosensweig and J. Popplewell, in *Electromagnetic Forces and Applications* (Elsevier Science, New York, 1992), p. 83.
[14] A. O. Tsebers, Magnetohydrodynamics **18**, 137 (1982).
[15] P. de Gennes and P. Pincus, Phys. Kondens. Mater. **11**, 189 (1970).
[16] G. Rushbrooke, G. Stell, and J. Hoye, Mol. Phys. **26**, 199 (1973).
[17] K. Sano and M. Doi, J. Phys. Soc. Jpn. **52**, 2810 (1983).
[18] K. I. Morozov, A. F. Pshenichnikov, Y. L. Raikher, and M. I. Shliomis, J. Magn. Magn. Mat. **65**, 269 (1987).
[19] Y. A. Buyevich and A. Ivanov, Physica A **190**, 276 (1992).

[20] V. I. Kalikmanov, Physica A **183**, 25 (1992).
[21] C. Joslin and S. Goldman, Mol. Phys. **79**, 499 (1993).
[22] H. Zhang and M. Widom, Phys. Rev. E **49**, 3591 (1994).
[23] A. Weinstein and S. Safran (unpublished).
[24] M. van Leeuwen, B. Smit, and E. Hendriks, Mol. Phys. **78**, 271 (1993).
[25] B. Smit, C. Williams, and E. Hendriks, Mol. Phys. **68**, 765 (1989).
[26] J. Powles, W. Evans, and N. Quirke, Mol. Phys. **46**, 1347 (1982).
[27] E. L. Pollock and B. J. Alder, Physica A **102**, 1 (1980).
[28] P. Kusalik, J. Chem. Phys. **93**, 3520 (1990).
[29] M. J. Stevens and G. S. Grest, following paper, Phys. Rev. E **51**, 5976 (1995).
[30] B. Groh and S. Dietrich, Phys. Rev. Lett. **72**, 2422 (1994); Phys. Rev. E **50**, 3814 (1994).
[31] S. W. de Leeuw, J. W. Perram, and E. R. Smith, Proc. R. Soc. London Ser. A **373**, 27 (1980).
[32] P. Kusalik, Mol. Phys. **81**, 199 (1994).
[33] R. B. Griffiths, Phys. Rev. **176**, 655 (1968).
[34] B. Smit, in *Computer Simulation in Chemical Physics*, edited by M. P. Allen and D. J. Tildesley (Kluwer Academic, Dordrecht, 1993), pp. 173–209.
[35] A. Panagiotopoulos, Mol. Sim. **9**, 1 (1992).
[36] P. C. Jordan, Mol. Phys. **25**, 961 (1973).
[37] P. C. Jordan, Mol. Phys. **38**, 769 (1979).
[38] J. Hansen and L. Verlet, Phys. Rev. **184**, 151 (1969).
[39] J. Israelachvili, *Intermolecular and Surface Forces* (Academic, New York, 1992).
[40] S. Fraden, A. Hurd, and R. Meyer, Phys. Rev. Lett. **63**, 2373 (1989).
[41] D. Krueger, IEEE Trans. Magn. **16**, 251 (1980).
[42] J. Liu, E. Lawrence, M. Ivey, and G. A. Flores (unpublished).
[43] M. Fermigier and A. Gast, J. Colloid Interface Sci. **154**, 522 (1992).
[44] Y. H. Hwang and X. l. Wu, Phys. Rev. E **49**, 3102 (1994).
[45] H. Zhang and M. Widom, J. Magn. Magn. Mat. **122**, 119 (1993).
[46] M. E. Fisher, J. Stat. Phys. **75**, 1 (1994).
[47] V. Russier and M. Douzi, J. Colloid Interface Sci. **162**, 356 (1994).
[48] J. B. Hayter, J. Chem. Soc. Faraday Trans. **87**, 403 (1991).
[49] J. Liu, T. Mou, and G. A. Flores (unpublished).

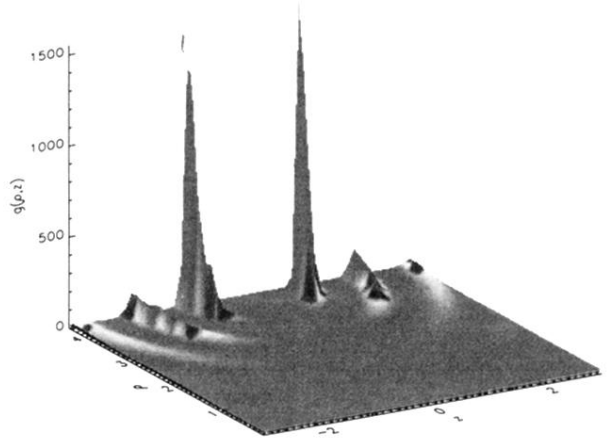

FIG. 4. The two-dimensional pair distribution function for $\mu^* = 3$ at $\rho^* = 0.01$ clearly displays the anisotropic structure of the fluid.